Journal of Ceramic Processing Research. Vol. 11, No. 6, pp. 673~677 (2010)

J O U R N A L O F
Ceramic Processing Research

Electrochemical characteristics of tin oxide and tin/tin oxide composite powder synthesized by aerosol flame deposition

Yeongap Kim, Yongsub Yoon and Dongwook Shin*
Division of Materials Science & Engineering, Hanyang University 17 Haengdang-dong, Seongdong-gu, Seoul 133-791, Korea

Aerosol flame deposition (AFD) was applied to synthesize nano-crystalline SnO_2 powder from an aqueous precursor solution of tin (IV) chloride. To produce Sn/SnO_2 composite powders, the synthesized SnO_2 powders were heat-treated under a 5% H_2 and 95% Ar mixed gas atmosphere at a temperature of 600 °C for 1-4 h. The XRD, XPS and SAED confirmed that the nano-crystalline SnO_2 and Sn/SnO_2 composites were well synthesized without any impurity phases. The amount of Sn in the composite was increased by increasing the heat treatment time. The Sn/SnO_2 composite heat-treated at a temperature of 600 °C for 1 h exhibited an improved cycling behavior compared to a pure SnO_2 anode with an initial capacity of 1476 mAh g^{-1} in the range of 0.01-1.2 V and maintained a reversible capacity above 327 mAh g^{-1} for more than 15 cycles.

Key words: Sn/SnO_2, Aerosol flame deposition (AFD), Li ion battery, Anode.

Introduction

Graphite is widely used as an anode in commercial cells due to its low cost, high yield and long cycle life. However, the capacity of graphite as a negative electrode has already approached the theoretical limit of LiC_6 (372 mAh g^{-1}). The search for new anode materials with high capacity and stable cyclic performance has been considered as a priority in the development of high energy density batteries [1-3]. In terms of Li^+ storage capacity, SnO_2 has been suggested as one of the most promising anode materials, because it can store more than twice as much Li^+ as graphite [4-6]. However, SnO_2 electrodes suffer from a severe volume change during lithium intercalation and de-intercalation, leading to pulverization and a quick fade of capacity [7]. As a result, this material has not been successfully applied in practical lithium ion batteries as yet. To overcome this problem, there have been many studies of combining Sn-based material with other materials to form composite electrodes with the intention to increase the dispersion of Sn-based oxide in another oxide matrix and/or on the surface [8-10]. A Sn/SnO_2 composite anode could be a plausible candidate in realizing increased reversible capacity as well as reduced irreversible capacity and capacity fade upon cycling, as this could increase the Sn : Li_2O ratio in the anode matrix. In this approach, the ratio between metallic Sn and SnO_2 is a critical factor for the optimum cyclic performance of the fabricated cell [11]. Therefore, to employ this material system for the anode of a battery, it is necessary to develop an adequate preparation process enabling nano-sized SnO_2 and Sn/SnO_2 composite powders to be made with precisely controlled Sn/SnO_2 ratios. Many routes have been applied to fabricate nano-sized SnO_2 particles, such as spray pyrolysis [9], a sol-gel method [12], chemical vapor deposition [13], magnetron sputtering [14], aerosol flame deposition [15], etc. Among these methods, the aerosol flame deposition (AFD) process is unique since it offers a vapor phase synthesis route to prepare powders from relatively inexpensive source material such as nitrates, carbonates, and chlorides. As pointed out in several previous reports [16-18], it is critical to prepare nano-sized powder to obtain reasonable cyclic performance in SnO_2 based anodes. Aerosol flame deposition is capable of synthesing nano-sized powder with appreciable productivity and quality.

In this study, SnO_2 and Sn/SnO_2 composite powders have been synthesized by an AFD technique and subsequent heat treatment. The resulting samples were characterized by X-ray diffraction (XRD), X-ray photoelectron spectroscopy (XPS), high-resolution transmission electron microscopy (HRTEM), and electrochemical measurements.

Experiments

Nanocrystalline SnO_2 powders were prepared by an aerosol flame deposition (AFD) technique. Schematically shown in Fig. 1 is the AFD system employed in this study. The experimental apparatus consists of an aerosol generator, a deposition chamber, and a gas delivery system. In the AFD process, a liquid precursor solution was prepared by dissolving the desired precursors into a solvent and then atomizing them into micro-sized droplets by an ultrasonic nebulizer. The precursor solution of tin was prepared by dissolving tin (IV) chloride (Aldrich, 99%) in methanol

*Corresponding author:
Tel : +82-2-2220-0503
Fax: +82-2-2220-4011
E-mail: dwshin@hanyang.ac.kr

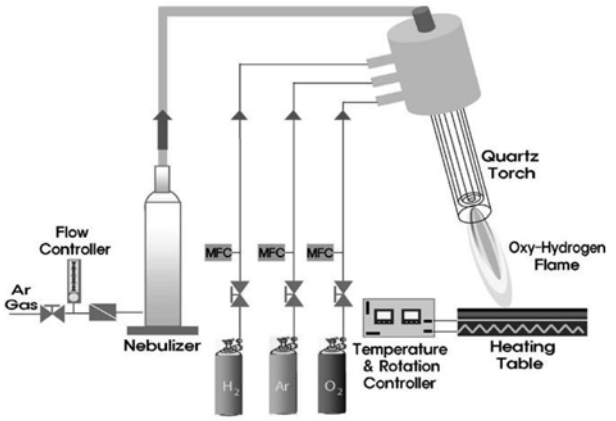

Fig. 1. A schematic diagram of the aerosol flame deposition system for the synthesis of SnO_2 nano-powder.

at a concentration of 0.1 mol and it was nebulized with an ultrasonic resonator (1.7 MHz). The aerosol generated by the ultrasonic nebulizer was subsequently carried into a flame made with the conditions of the oxygen flow rate of 7.5 L·minute^{-1}, Ar shield flow rate of 3 L·minute^{-1}, and hydrogen flow rate of 3 L·minute^{-1}. Subsequently, the as-synthesized SnO_2 powders were heat-treated under a 5% H_2 and 95% Ar mixed gas atmosphere at a temperature of 600 °C for 1-4 h in order to convert to Sn/SnO_2 composite powders.

The as-prepared samples were characterized by X-ray diffractometer (XRD ; Rigaku D/max-2500, with Cu K_{α}. X-ray radiation 40 mA 100 mV), X-ray photoelectron spectroscopy (XPS; VG Multilab ESCA 2000 system with an Al K_{α}. X-ray source 1486.6 eV), high-resolution transmission electron microscopy (HRTEM), and selected area electron diffraction (HRTEM/SAED ; JEOL, JEM-2100F). For electrochemical performance evaluation, half-cell studies were performed. The working electrodes consisted of active materials, acetylene black and IPA(Iso propyl alchole) on copper foil. The resulting paste was pressed about at 20 MPa and then dried at 120 °C under a vacuum for 24 h. The cells were assembled in an argon-filled glove box. The galvanostatic charge/discharge tests were examined via CR2032 coin-type cells with lithium metal counter electrodes, Celgard 2400 membrane separators and an electrolyte of 1M $LiPF_6$ in a mixture of ethylene carbonate (EC) and dimethyl carbonate (DMC) (1 : 1 by volume) at an ambient temperature on a multi-channel battery tester system (WBCS 3000) in the voltage range from 0.01 to 1.2 V versus Li/Li$^+$ at a current density of 30 mA g^{-1}.

Results and Discussion

The nanocrystalline SnO_2 powder was obtained by the AFD technique in the optimum synthesis conditions. Fig. 2 shows the XRD patterns of the nanocrystalline SnO_2 powder and the Sn/SnO_2 composite powders. As can be seen in Fig. 2(a), the diffraction peak positions were in good

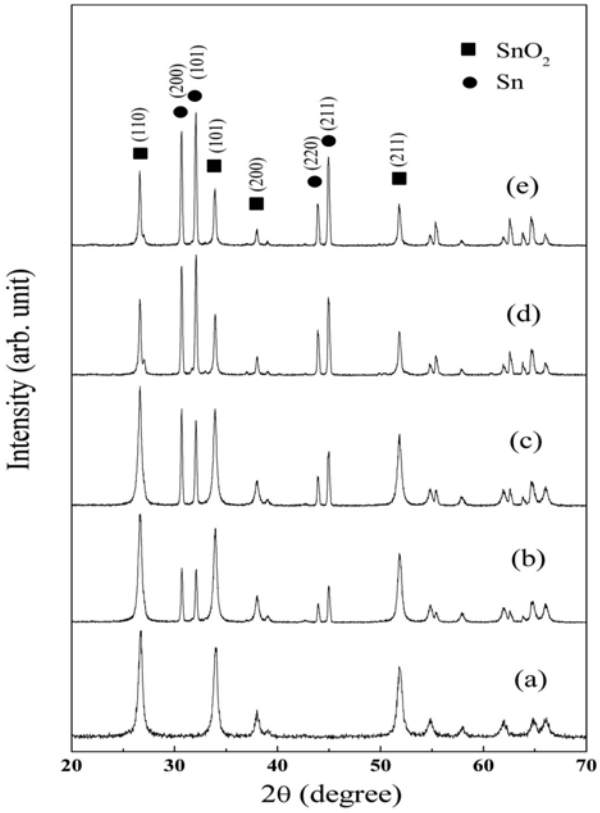

Fig. 2. X-ray diffraction patterns of (a) as-prepared SnO_2, and heat-treated at 600 °C for (b) 1 h, (c) 2 h, (d) 3 h, and (e) 4 h.

agreement with that of cassiterite SnO_2 (JCPDS No. 41-1445) and no impurity peaks were detected. Fig. 2(b, c, d, and e) show the effect of heat treatment on the synthesized SnO_2 powder. The peaks corresponding to the major constituents in the compound dominate in the patterns. The diffraction peak positions were in good agreement with those of cassiterite SnO_2 (JCPDS No. 41-1445) and metallic Sn (JCPDS No. 86-2265). From the XRD patterns, one can see that the intensity of the SnO_2 peaks was slightly decreased, while that of the Sn peaks was an increase in with increasing the heat treatment time. It is clear that heat-treatment in the reducing atmosphere reduced SnO_2 to Sn. To obtain more information on the chemical states of the Sn/SnO_2 composite powders, XPS analysis was performed. Fig. 3 shows the vicinity of the Sn 3d peaks from the synthesized Sn/SnO_2 composite powders after heat treatment for various times. The Sn $3d_{5/2}$ spectrum has a main peak at approximately 487 eV which corresponds to SnO_2 and other oxidation states as well as a shoulder at approximately 485 eV which corresponds to metallic Sn [19]. These results indicate that the SnO_2 powder is partially reduced after heat treatment under a reducing atmosphere. The peak intensity of SnO_2 (Sn^{4+}) was decreased while that of Sn metal (Sn^0) was increased with an increase in the heat treatment time. These results are in good agreement with the XRD results shown in Fig. 2.

The morphology, particle size, and microstructure of

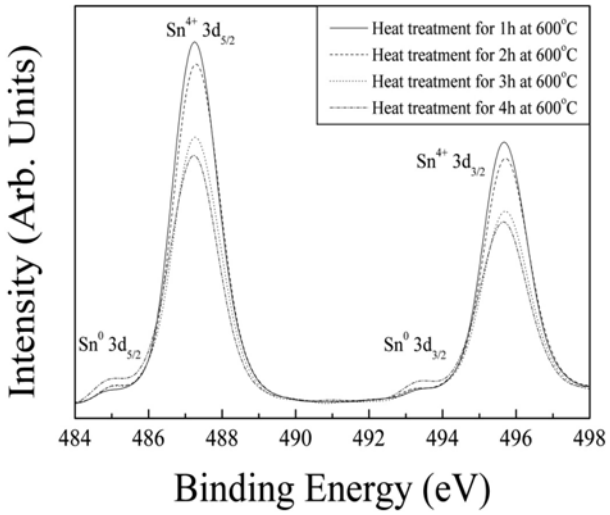

Fig. 3. The Sn 3d core level XPS spectra of Sn/SnO_2 composite powders produced by heat treatment of SnO_2 powder at 600 °C for various times.

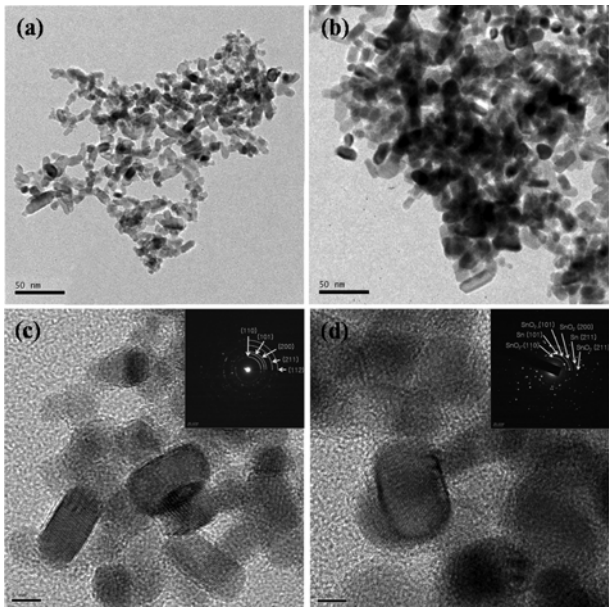

Fig. 4. TEM and HRTEM images of (a) and (c) as-prepared SnO_2, (b) and (d) Sn/SnO_2 composite by heat-treatment at 600 °C for 4 h. The insets at the top right of (c) and (d) are the selected area electron diffraction (SAED) patterns.

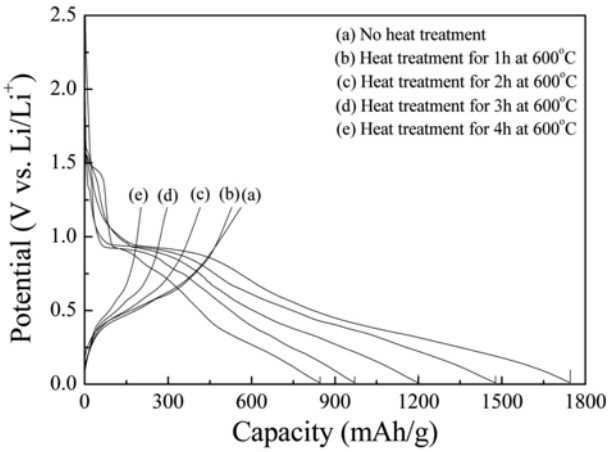

Fig. 5. The first discharge/charge curves of the SnO_2 and Sn/SnO_2 composite anodes by heat-treatment at 600 °C for 1-4 h (constant current density of 30 mA g^{-1}, with voltage limit set at 0.01-1.2 V vs. Li/Li^+).

the SnO_2 and Sn/SnO_2 composite powders were observed by TEM and HRTEM. Fig. 4(a) and (b) show typical TEM images of the as-prepared SnO_2 and Sn/SnO_2 composite powder after heat-treatment at 600 °C for 4 h. Each sample is composed of nano-sized particles with a round morphology and narrow size distribution. The average particle size is zin the range of 5-15 nm when estimated visually from the TEM images. The particle size of Sn/SnO_2 composite powders formed by heat-treatment was not substantially increased and the powders became slightly agglomerated. Fig. 4(c) and (d) shows the high-resolution TEM images of the as-prepared SnO_2 and Sn/SnO_2 composite powder after heat-treatment at 600 °C for 4 h, and the insets in Fig. 4(c) and (d) and the selected area electron diffraction (SAED) patterns. As reported in Fig. 4(c) and (d), each sample is indeed polycrystalline, comprising numerous nanocrystallites with sizes of 5-15 nm, similar to the sizes seen in Fig. 4(a) and (b). As shown in Fig. 4(c), the selected area electron diffraction pattern (inset) indicates that the SnO_2 nanoparticles are mostly in single crystalline state. Selected area electron diffraction (SAED), proved that the SnO_2 had a polycrystalline structure and the polycrystalline rings could be ascribed to the (110), (101), (200), (211), and (112) diffraction planes of the tetragonal rutile like SnO_2. Fig. 4(d) shows the formation of tetragonal Sn with different lattice fringes of (101) and (211) planes, corresponding to spacings of 2.79 and 1.99 Å, respectively. The diffraction pattern also confirms the formation of SnO_2 and tetragonal Sn, as shown in the inset. This result is in good agreement with the XRD and XPS results.

The properties of the SnO_2 and the Sn/SnO_2 composite as anodes for a lithium-ion rechargeable battery were studied using constant current charge/discharge measurements. Fig. 5 shows the first discharge and charge curves of the SnO_2 and Sn/SnO_2 composite electrodes at a constant current density of 30 mA g^{-1} between 0.01 and 1.2 V. As seen in Fig. 5, during the first reduction, the plateau observed at about 0.8 and 0.9 V can be assigned to the formation of solid-electrolyte interface (SEI) layers on the surface of the SnO_2 and reduction of SnO_2, which lead to the formation of amorphous Li_2O and metallic Sn. The formation of Li_2O is an irreversible reaction leading to the initial irreversible capacity of these electrodes. Further reaction of the newly formed metallic Sn with lithium subsequently leads to the formation of Li-Sn alloys with the composition, $Li_{4.4}Sn$. The formation of Li_xSn alloys and lithium intercalation occur below 0.75 V. The electrochemical reaction mechanism of SnO_2 with a lithium-ion is generally described as follows [5]:

$$SnO_2 + 4Li^+ + 4e^- \rightarrow Sn + 2Li_2O \quad (1)$$

$$Li^+ + xe^- + Sn \leftrightarrow Li_xSn \qquad (0 \le x \le 4.4) \qquad (2)$$

The maximum theoretical capacity is estimated to be 781 mAh g^{-1} according to the alloying and de-alloying mechanism. The plateau assigned to the formation of the amorphous Li_2O phase for the Sn/SnO_2 composite electrode by heat-treatment at 600 °C for 4 h became shorter than that of the other electrodes, because of the increased content of Sn in the composites. This result indicates that the addition of Sn may reduce the formation of amorphous Li_2O for the Sn/SnO_2 composite electrodes. Hence an addition of Sn could reduce the irreversible capacity, and improve the cyclability. However, the irreversible capacity as well as the reversible capacity were decreased when the content of Sn in the composite were increased. The reason why the reversible capacity decreases is that the particle size of Sn/SnO_2 composites became more agglomerated and grew to larger sizes with an increase in the heat treatment time. Kim *et al*. [16] and Mukaibo *et al*. [20] have reported the effect of particle size on the cycle performance. Smaller particles have larger surface areas, which would make the diffusion for the Li^+ into the active element easier for the Sn-Li alloying reaction, leading to a higher reversible capacity. This could contribute to the lightening of stress caused by the volume change during the substantial charge and discharge, and suppress the degradation of the electrode.

The initial discharge capacities were 1744, 1476, 1180, 968 and 843 mAh g^{-1} for the SnO_2 and the Sn/SnO_2 composite powders heat-treated at 600 °C for 1-4 h, respectively, which all exceed the theoretical capacity of SnO_2. The initial coulombic efficiencies of these electrodes are 35.6, 38.0, 37.7, 32.5, and 25.2%, respectively.

The electrochemical cyclic properties of the SnO_2 and Sn/SnO_2 composite electrodes over 15 cycles are compared in Fig. 6. In terms of cyclability, the initial discharge capacity decreased to 259, 327, 269, 175, and 90 mAh g^{-1} after 15 cycles, corresponding to 14.8, 22.2, 22.8, 18.1, and 10.7% retention of the initial capacity for SnO_2 and Sn/SnO_2 composite anode heat-treated at 600 °C for 1-4 h, respectively. It can be seen that although the capacities decrease with an increase in the amount of Sn amount in the composites the cycle efficiencies remain higher for Sn/SnO_2 composite electrodes. This could be ascribed to the creation of Sn on the surface of SnO_2, which is beneficial to the utilization of Sn and the release of the stress caused by the drastic volume variation during the lithium alloying/dealloying process.

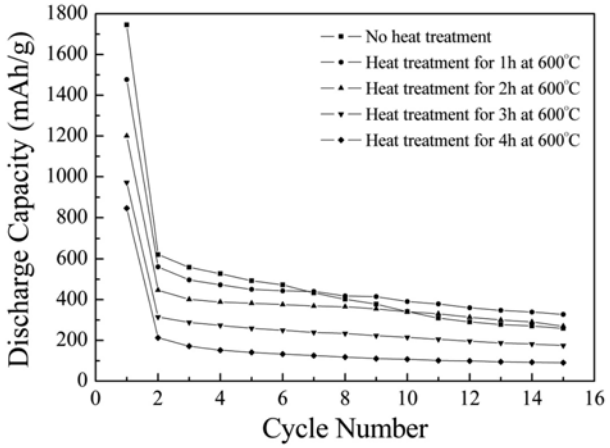

Fig. 6. Cyclic performance of SnO_2 and Sn/SnO_2 composite anodes in the 0.01-1.2 V (vs. Li/Li^+) voltage window at a constant current density of 30 mA g^{-1}.

Conclusions

Nanocrystalline SnO_2 powder was synthesized by aerosol flame deposition from an aqueous solution of tin (IV) chloride ($SnCl_4$) and methanol (CH_3OH). A subsequent heat-treatment process at 600 °C for 1-4 h under a reducing atmosphere successfully produced crystalline Sn/SnO_2 composite powders. XRD, XPS, and TEM analysis confirmed the formation of metallic Sn. The Sn/SnO_2 composite by heat-treated at 600 °C for 1 h exhibited better cyclability over 15 cycles than did SnO_2 and the other Sn/SnO_2 composites. It appears that the formation of Sn on the surface of SnO_2 is a benefit to reduce the irreversible capacity and improve the cyclability.

Acknowledgements

This work was supported by the Seoul Research and Business Development Program (Grant No. 10583). Also, it is partially supported by the Manpower Development Program for Energy & Resources supported by the Ministry of Knowledge and Economy (MKE).

References

1. J.M. Tarascon and M. Armand, Nature 414 (2001) 359-367.
2. J.R. Dahn, T. Zheng, Y. Liu and J. S. Xue, Science 270 (1995) 590-598.
3. M. Winter, J.O. Besenhard, M.E. Spahr and P. Novak, Adv. Mater. 10 (1998) 725-763.
4. Y. Idota, T. Kubota, A. Matsufuji, Y. Maekawa and T. Miyasaka, Science 276 (1997) 1395-1397.
5. I.A. Courtney and J.R. Dahn, J. Electrochem. Soc. 144 (1997) 2045-2052.
6. J.O. Besenhard, J. Yang and M. Winter, J. Power Sources 68 (1997) 87-90.
7. T. Brousse, R. Retoux, U. Herterich and D.M. Schleich, J. Electrochem. Soc. 145 (1998) 1-4.
8. S.T. Chang, L.C. Leu and M.H. Hon, J. Alloys compd. 403 (2005) 335-340.
9. L. Yuan, K. Konstantinov, G.X. Wang, H.K. Liu and S.X. Dou, J. Power Sources 146 (2005) 180-184.
10. J. Sarradin, N. Benjelloun, G. Taillades and M. Ribes, J. Power Sources 97/98 (2001) 208-210.
11. A. Sivashanmugam, T. Prem Kumar, N.G. Renganathan, S. Gopukumar, M. Wohlfahrt-Mehrens and J. Garche, J. Power Sources 144 (2005) 197-203.
12. H. Li, X. Huang and L.Chen, J. Power Sources 81/82 (1999) 335-339.
13. R.D. Tarey and T.A. Raju, Thin Solid Films 128 (1985)

181-189.
14. T. Minami, H. Nanto and S. Takata, Jpn. J. Appl. Phys. 27 (1988) 287-289.
15. Y.G. Kim, Y.S. Yoon and D.W. Shin, J. Anal. Appl. Pyrolysis 85 (2009) 557-560.
16. C.J. Kim, M.J. Noh, M.S. Choi, J.P. Cho and B.W. Park, Chem. Mater. 17 (2005) 3297-3301.
17. L. Yuan, Z.P. Guo, K. Konstantinov, H.K. Liu and S.X. Dou, J. Power Sources 159 (2006) 345-348.
18. H.J. Ahn, H.C. Choi, K.W. Park, S.B. Kim and Y.E. Sung, J. Phys. Chem. B 108 (2004) 9815-9820.
19. D. Briggs and M. P. Seah, in "Practical Surface Analysis, vol. 1: Auger and X-ray Photoelectron Spectroscopy, 2nd edn." (Wiley, 1990) p. 642.
20. H. Mukaibo, A. Yoshizawa, T. Momma and T. Osaka, J. Power Sources 119/121 (2003) 60-63.